Efficient Finite Element Method to Estimate Eddy Current Loss due to Random Interlaminar Contacts in Electrical Sheets

INTERNATIONAL JOURNAL OF NUMERICAL MODELLING: ELECTRONIC NETWORKS, DEVICES AND FIELDS

Int. J. Numer. Model. 2017; **00**:2–18

Published online in Wiley InterScience (www.interscience.wiley.com). DOI: 10.1002/jnm

Efficient Finite Element Method to Estimate Eddy Current Loss due to Random Interlaminar Contacts in Electrical Sheets

S.B. Shah*[1], P. Rasilo [1,2], H. Hakula [3] and A. Arkkio [1]

Department of Electrical Engineering and Automation, Aalto University, P.O Box 13000, FI-00076 Aalto, Finland [1]

Department of Electrical Engineering, Tampere University of Technology, P.O Box 692, FI-33101 Tampere, Finland [2]

Department of Mathematics and Systems Analysis, Aalto University, P.O Box 13000, FI-00076 Aalto, Finland [3]

SUMMARY

Electrical sheets of electrical machines are laminated to reduce eddy current loss. However, a series of punching and pressing processes form random galvanic contacts at the edges of the sheets. These galvanic contacts are random in nature and cause an additional eddy current loss in the laminated cores. In this paper, a stochastic Galerkin finite element method is implemented to consider random interlaminar contacts in the magnetic vector potential formulation. The random interlaminar conductivities at the edges of the electrical sheets are approximated using a conductivity field and propagated through the finite element formulation. The spatial random variation of the conductivity causes the solution to be random and hence it is approximated by using a polynomial chaos expansion method. Finally, the additional eddy current losses due to the interlaminar contacts are estimated from a stochastic Galerkin method and compared with a Monte Carlo method. Accuracy and computation time of both models are discussed in the paper. Copyright © 2017 John Wiley & Sons, Ltd.

Received ...

KEY WORDS: Eddy current; finite element analysis; Monte Carlo method; polynomial chaos expansion; random field; uncertainity quantification.

1. INTRODUCTION

Punching and pressing of electrical sheets form burrs and deteriorate the magnetic properties at the edges of electrical sheets. These burrs also deteriorate the insulation of adjacent sheets and make random galvanic contacts between the sheets [1, 2]. There are both experimental and analytical approaches to model the interlaminar short circuits of lamination stacks [3, 4]. In [5, 6] artificial galvanic contacts are applied to the opposite sides of a transformer limb, and additional losses are quantified through a measurement. However, the interlaminar galvanic contacts are random in nature and introduce uncertainties in the electromagnetic field solution. There are different stochastic models developed in the literature to account for uncertainties in numerical models, but these studies are mostly related to the fields of mechanical and civil engineering. Uncertainties in the model geometry and different stochastic methods are discussed in [7, 8, 9, 10, 11]. In the field of electromagnetism, stochastic studies are ongoing, and there are some studies done to quantify the uncertainties introduced in the magnetic properties of electrical sheets due to manufacturing effects [12, 13]. A stochastic model was proposed to take into account the uncertainty in the reluctivity due to the manufacturing process in the case of a slinky stator through experiment [14, 15, 16]. This stochastic behavior of magnetic properties is used as the input in stochastic finite element models [17] to study the variability in the losses of an electrical machine. Similarly, different stochastic methods are considered in [9] and the 3-dimensional spectral stochastic finite element method is tested for electrostatics applications with random permittivity.

In stochastic models, the uncertain data is treated as a random variable defined on a proper probability space. The solutions of those models are also random in nature, and typically these solutions are used to obtain statistical information about the physical system. Often, in the field

*Correspondence to: S.B. Shah, Department of Electrical Engineering and Automation, Aalto University, P.O Box 13000, FI-00076 Aalto, Finland. Email: sahas.bikram.shah@aalto.fi

Contract/grant sponsor: FP7/2007-2013 ERC; contract/grant number: 339380

†Please ensure that you use the most up to date class file, available from the JNM Home Page at

http://www3.interscience.wiley.com/journal/4673/home

Prepared using jnmauth.cls

DOI: 10.1002/jnm

of engineering application, the mean and the variance are the interesting properties. The first step in solving the stochastic models is to parametrize the stochastic input. The stochastic input can be characterized by either a finite number of system parameters or a random field depending upon the physical system. In the case of a finite number of system parameters, the parametrization can be done by the random variables. Often, for the Gaussian parameter, a Cholesky decomposition of their covariance matrix is done, and for non-Gaussian parameters, a Rosenblatt transformation is performed [18]. A Monte Carlo method is a successful statistical technique to approximate the output response with the stochastic input. It employs repetitive tests over a sufficiently large body of sampling and is extensively used to validate the different stochastic methods. Such method was implemented in [19] to study the effect of inter-laminar contacts on electromagnetic losses of an induction machine. However, this can be very time consuming and computationally expensive depending upon the convergence rate.

In this paper, the uncertainty introduced due to the formation of burrs during the manufacturing process of the electrical sheets is modeled by considering the conductivity at the edges of the electrical sheets as a random field. The conductivity field is a list of random numbers whose indices are mapped into the burred region. The burred region formed by the random galvanic contacts between the electrical sheets is shown in Figure 1. Often, the Karhunen-Loeve (KL) expansion is employed to represent the random conductivity field as an infinite linear combination of orthonormal eigenfunctions of the corresponding covariance operator. These non-statistical methods are widely used for uncertainty quantification. Similarly, other methods are studied in the literature. The perturbation method is used in determining the first and second order moments which are expansions of random quantities around their mean values [20, 21, 22]. The Neumann expansion is a method where the coefficients are expanded into Neumann series, but this method has low convergence rate [23, 24].

An alternative approach is a spectral method in which the statistical properties are approximated as a sum of certain basis functions and deterministic coefficients. The spectral method also has two categories, intrusive and non-intrusive approaches. The non-intrusive method employs some specific

Prepared using jnmauth.cls
DOI: 10.1002/jnm

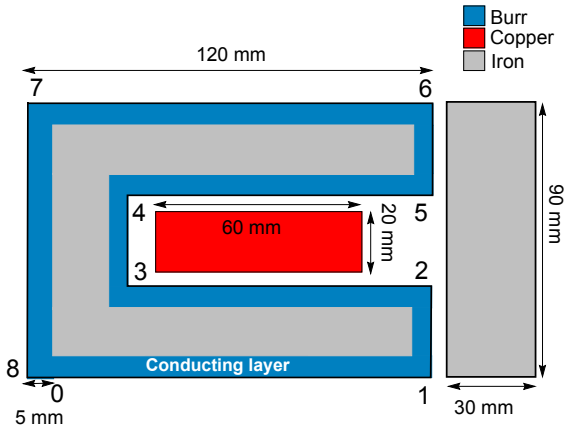

Figure 1. Schematic of UI type electrical sheets showing periodic indices and conducting domains.

values or numbers of realizations to approximate statistical moments such as mean and standard deviation. The intrusive or Galerkin method introduces some suitable space or basis of polynomials and looks for surrogates for which the residual is orthogonal to that space in an appropriate sense [25]. In the ideal case, the Galerkin approach produces more accurate solutions than the non-intrusive method. The Galerkin method requires a modification to the current deterministic solver and is thus more tedious to work with than the non-intrusive methods [26]. However, the numerical methods suggest that the Galerkin approach has a high potential for large-scale analyses, so we afford to make that extra investment. Hence, for the sake of development of the accurate method, quasi-magnetostatic analysis of UI type electrical sheets is considered [1].

2. METHODS

2.1. Model formulation

The edges of the UI type electrical sheets are deteriorated due to punching, and random burrs are formed. These burrs will form the interlaminar contacts. It is assumed that these contact layers have the width of 5 mm for the sake of development of the model as shown in Figure 2. The interlaminar contacts of UI electrical sheets are modeled using the magnetic vector potential and electric scalar

Prepared using jnmauth.cls
DOI: 10.1002/jnm

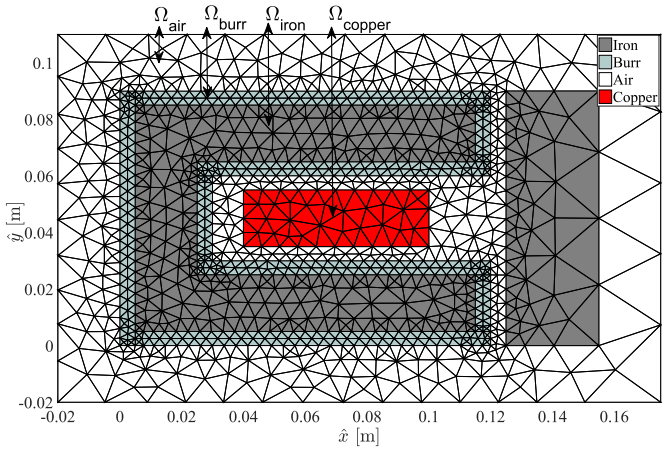

Figure 2. A first order triangular finite element mesh.

potential formulation [27] as given by

$$\nabla \times (\nu \nabla \times \boldsymbol{A}) + \sigma \frac{\partial \boldsymbol{A}}{\partial t} + \sigma \nabla \phi = \boldsymbol{J}_{\mathrm{s}} \tag{1}$$

where ν, $\boldsymbol{A}$, σ, ϕ are the reluctivity, magnetic vector potential, conductivity and electric scalar potential, respectively. In 2D problems, if the source current density has only z component then the magnetic vector potential also has only z component, i.e. $\boldsymbol{J}_{\mathrm{s}} = J_{\mathrm{s}}\mathbf{e}_{\mathrm{z}}$ and $\boldsymbol{A} = A\mathbf{e}_{\mathrm{z}}$. The $\nabla\phi$ term which comes from the irrotational part due to electric charges and the polarization of dielectric materials has only a z component since J_{s} and A are in that direction. The assumption of two-dimensionality does not allow potential difference due to electric charges and the polarization of dielectric materials. Thus, the exact solution of the scalar potential ϕ is not needed in the burred regions [27]. In the two-dimensional case, Coulomb's gauge is satisfied automatically and considering linear material, the partial differential equation (1) becomes,

$$-\nu \nabla^2 A + \sigma \frac{\partial A}{\partial t} = J_{\mathrm{s}}, \text{ on } \Omega = \Omega_{\mathrm{iron}} \cup \Omega_{\mathrm{air}} \cup \Omega_{\mathrm{burr}} \cup \Omega_{\mathrm{copper}}, \tag{2}$$

where Ω is the region under study. It can be assumed that in any current carrying region, there is either a source current density J_{s}, but no eddy current density (i.e. $\sigma = 0$) or an eddy current density (i.e. $\sigma \neq 0$), but no source current density. The equations that are solved in different regions are

Prepared using jnmauth.cls
DOI: 10.1002/jnm

given as

$$\begin{aligned} -\nu\nabla^2 A &= 0, \text{ on } \Omega_{\text{iron}}, \\ -\nu_0\nabla^2 A &= 0, \text{ on } \Omega_{\text{air}}, \\ -\nu\nabla^2 A + \sigma\frac{\partial A}{\partial t} &= 0, \text{ on } \Omega_{\text{burr}}, \\ -\nu_0\nabla^2 A &= J_{\text{s}}, \text{ on }, \Omega_{\text{copper}}, \end{aligned} \tag{3}$$

where ν_0 is the reluctivity of air. Ω_{iron}, Ω_{air}, Ω_{burr}, Ω_{copper} are the iron region, air region, conducting region and current source region, respectively. The UI type electrical sheets are spatially discretized using first order triangular elements. Each node of a triangular element constitutes three degrees of freedom. The total number of nodes obtained is 1154, and the Dirichlet boundary condition is imposed on the outer boundaries of air. The random conductivity is propagated through the mathematical model (2) and the response of random conductivity is obtained from the solution of the vector potential. The interlaminar eddy current loss is calculated in post-processing from the obtained solution. The two-dimensional and low-frequency assumptions allow studying the effect of random galvanic contacts along the boundary edges of electrical steels in the field solution. However, if the interlaminar contacts are present inside the electrical sheets then each laminate can be resolved as in [28] and the electromagnetic field solution inside the stack can be obtained. In such cases, the effect of random interlaminar contacts can be studied using a two-dimensional approximation of the random conductivity field.

2.2. Stochastic formulation

2.2.1. Uncertainty quantification The random conductivities at the burred region of the UI type sheets are approximated as a conductivity field. Often, the conductivity field is approximated as a spectral decomposition of its autocovariance function, and eigenvalues, as well as eigenfunctions, are solved. In this case, the random conductivities are approximated by a one-dimensional conductivity field. It has been studied in [2, 6, 19] that burrs are more likely to occur at the edges of electrical sheets and the burr width is relatively small. Hence, the random conductivities are approximated by a one-dimensional conductivity field, meaning that the interlaminar random

Prepared using jnmauth.cls
DOI: 10.1002/jnm

conductivity field is varying only along the edges of the electrical sheets. The conductivity along the burr width is considered to be constant. The conductivity field will be used within the blue colored region in Figure 1 along the edge of the electrical sheet. The variations of the conductivity field depends on the covariance function. The finite dimensional approximations of the covariance function start by limiting the span of the data, for example, Mercers theorem assumes that the data extends over a small domain and Nystroms approximation assumes the data is distributed according to the covariance function [29]. In the case of the restricted domain, the covariance function or the kernel can be made periodic by making copies of it with period Λ and a finite approximation of the covariance function can be obtained from its Fourier spectrum [30]. In this case, the periodic length of eight is considered since there are eight restricted domains. The basis of the periodic covariance function is given as (4) where $L = \frac{2\pi}{\Lambda}$, x is the spatial position and σ_i is the discrete spectrum [31]. The orthogonality nature and the smoothness of sine and cosine basis functions improve the convergence rate to approximate the covariance function [32].

$$\Psi_i(\mathrm{x}) = \begin{cases} \sigma_{\frac{i}{2}} \sin(\frac{i}{2} L\mathrm{x}) & i > 0 \text{ even}, \\ \sigma_{\frac{i+1}{2}} \cos(\frac{i+1}{2} L\mathrm{x}) & i > 0 \text{ odd}. \end{cases} \tag{4}$$

Hence, the conductivity field is given by

$$\sigma(\mathrm{x}, \zeta) = \sigma_0 + \sum_{i=1}^{\mathrm{M}} \Psi_i(\mathrm{x})\zeta_i. \tag{5}$$

Here σ_0 is the mean value of the conductivity, and ζ_i are the independent random variables from a beta distribution with parameters $\alpha = 12, \beta = 2$. The conductivity distribution was assumed to be a beta distribution based on theoretical arguments and experimental observations [33]. The conductivity is a non-negative quantity which is ensured by maximization,

$$\sigma_0 \geq \underbrace{-\sum_{i=1}^{\mathrm{M}} \Psi_i(\mathrm{x})\zeta_i}_{\mathrm{Max}}, \quad \sigma(\mathrm{x}, \zeta) \geq 0. \tag{6}$$

The number of random variables to approximate the conductivity field depends upon the number of M expansion terms. The conductivity field is varying according to the position, and the covariance function of the conductivity field at the same position is unity. Hence, the number of expansion

Prepared using jnmauth.cls
DOI: 10.1002/jnm

terms is determined by minimizing the error of the exact covariance function and the approximated covariance function. The approximated covariance function is calculated according to,

$$\mathrm{Cov}(\mathrm{x}, \mathrm{x}') = \sum_{i=1}^{\mathrm{M}} \Psi_i(\mathrm{x})\Psi_i(\mathrm{x}'). \tag{7}$$

The number of expansion terms, however, depends on how the conductivities are correlated to each other. The number of expansion terms M is determined based on the minimum error of the covariance function of the conductivity field as shown in Figure3. The exact covariance function,

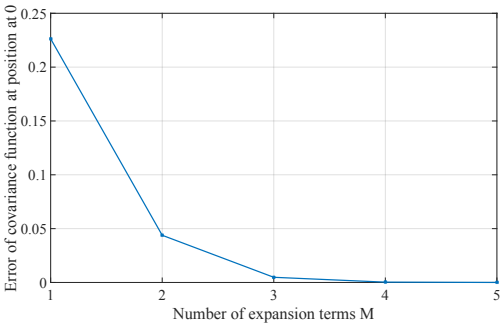

Figure 3. Approximation error at different parameters of M.

and the solution difference of the approximated and the exact covariance functions are shown in Figure 4a and Figure 4b, respectively. The conductivity field as a function of periodic length is shown in Figure 5. The conductivity values of each domain are mapped from these periodic conductivity fields. The conductivity value at each integration points during the finite element assembly is obtained by mapping the integration point first into its global spatial coordinate, and then the conductivity value is obtained from the conductivity field depending on its domain and periodicity. For instance, the conductivity value in first domain of Figure 1 along 0→1 is obtained as, $\sigma(\frac{\hat{x}}{l_1})$ and second domain along 1→2 is obtained as $\sigma(\frac{\hat{y}}{l_2} + 1)$, where $\hat{x}$ and $\hat{y}$ are the spatial coordinates. Similarly, the conductivity values of all other domains are obtained.

2.2.2. Stochastic Galerkin Finite Element Method (SGFEM) The inclusion of random conductivities makes the solution of (2) to be random. Hence, the uncertain nodal magnetic vector potential is approximated using Jacobi polynomials (ψ) as given in (8). The size P of the polynomials in the chaos expansion is provided by (9), where M is the number of expansion terms in conductivity

Prepared using jnmauth.cls
DOI: 10.1002/jnm

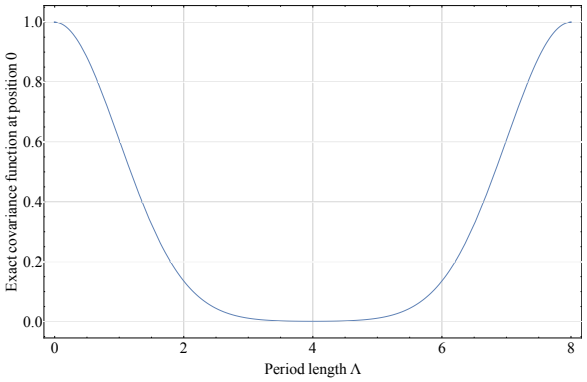

(a) Exact covariance function

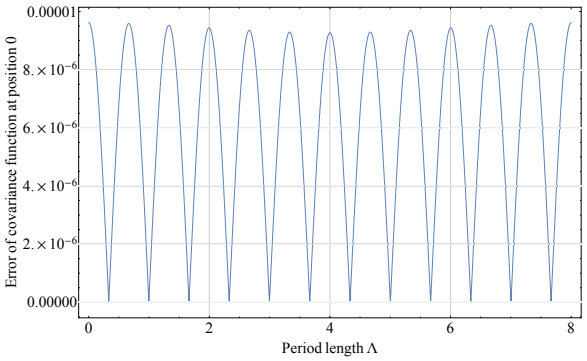

(b) Absolute error between exact and approximate covariance function

Figure 4. Error of conductivity expansion at M = 5

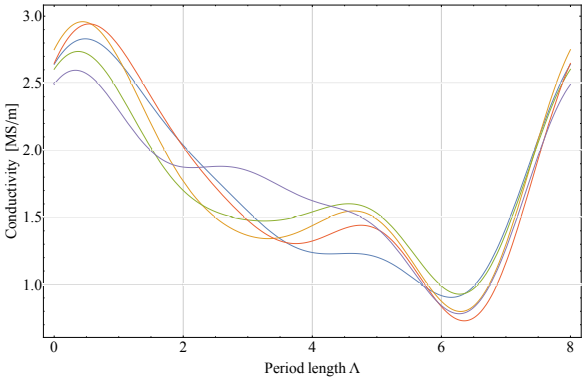

Figure 5. Random conductivity field along the burred region.

field expansion and p is the order of the Jacobi polynomials. The choice of polynomials depends on the orthogonality relations to a probability distribution. The orthogonality relation of polynomials

Prepared using jnmauth.cls
DOI: 10.1002/jnm

and probability distributions is listed in Table 1.

$$\boldsymbol{a} = \sum_{j=0}^{\text{P-1}} \boldsymbol{a}_j \psi_j(\zeta_i(\theta)_{i=1}^{\text{M}}) \tag{8}$$

$$\text{P} = \frac{(\text{p}+\text{M})!}{\text{p!M!}} \tag{9}$$

Equation (2) is discretized in space and then substituting (5) in (2) and applying the Galerkin

Table I. Probability distributions and weight functions [32]

Orthogonal polynomial family	Probability distribution function
Hermite	Normal
Jacobi	Beta
Legendre	Continous uniform
Laguerre	Gamma

method associated with the finite element method yields a system of equations,

$$\boldsymbol{S}\boldsymbol{a} + \boldsymbol{T}\frac{\mathrm{d}\boldsymbol{a}}{\mathrm{d}t} = \boldsymbol{f}. \tag{10}$$

The entries of the matrices $\boldsymbol{S}$, $\boldsymbol{T}$ and $\boldsymbol{f}$ are given by

$$\begin{aligned} [\boldsymbol{S}]_{\text{n}\times\text{n}} &= \int_\Omega \nu(\nabla \boldsymbol{N}^{\text{T}}) \cdot (\nabla \boldsymbol{N}) \mathrm{d}\Omega, \\ [\boldsymbol{T}]_{\text{n}\times\text{n}} &= \int_\Omega \sigma(\text{x},\zeta) \boldsymbol{N}^{\text{T}} \boldsymbol{N} \mathrm{d}\Omega, \\ [\boldsymbol{f}]_{\text{n}\times 1} &= \int_\Omega J_{\text{s}} \boldsymbol{N} \mathrm{d}\Omega, \end{aligned} \tag{11}$$

where n is the total number of nodes in the entire domain (Ω) and $\boldsymbol{N}$ is the shape function of the first order triangular element. The current density J_{s} is considered varying sinusoidally with time at low angular frequency ω so the vector potential also varies sinusoidally. The time derivative of the vector potential is replaced with $\text{j}\omega$ to derive (12) from (10).

$$\boldsymbol{S}\boldsymbol{a} + \text{j}\omega\boldsymbol{T}\boldsymbol{a} = \boldsymbol{f} \tag{12}$$

Prepared using jnmauth.cls
DOI: 10.1002/jnm

The random conductivity field is in the matrix $\boldsymbol{T}$ so as the first level of assembly, the mean and weighted global $\boldsymbol{T}$ matrix is collected after the expansion of conductivity $\sigma(\mathrm{x},\zeta)$. It is given by

$$\begin{aligned}[\bar{\boldsymbol{T}}]_{\mathrm{n}\times\mathrm{n}} &= \int_{\Omega} \sigma_0 \boldsymbol{N}'\boldsymbol{N}\mathrm{d}\Omega,\\ [\bar{\boldsymbol{T}}_i]_{\mathrm{n}\times\mathrm{n}} &= \sum_{i=1}^{\mathrm{M}} \int_{\Omega} \Psi_i(\mathrm{x})\zeta_i \boldsymbol{N}'\boldsymbol{N}\mathrm{d}\Omega.\end{aligned} \tag{13}$$

The vector potential is approximated using (8), and the Galerkin method associated with SGFEM is implemented to the matrix $\boldsymbol{T}$ and finally, it is written as,

$$\begin{aligned}\sum_{i=0}^{\mathrm{M}}\sum_{j=0}^{\text{P-1}} \mathbf{c}_{ijk}(\boldsymbol{S}_i + \mathrm{j}\omega\boldsymbol{T}_i)\cdot\boldsymbol{a}_j &= \boldsymbol{F}_k,\\ \boldsymbol{L}_{jk} = \mathbf{c}_{0jk}(\boldsymbol{S} + \mathrm{j}\omega\bar{\boldsymbol{T}}) + \mathrm{j}\omega\sum_{i=1}^{\mathrm{M}}\sum_{j=0}^{\text{P-1}} \mathbf{c}_{ijk}\boldsymbol{T}_i,&\\ j,k = 0,\cdots,\mathrm{P}-1,&\\ \mathbf{c}_{ijk} = \mathbf{E}[\zeta_i\psi_j\psi_k],&\\ \boldsymbol{F}_k = \mathbf{E}[f\psi_k].&\end{aligned} \tag{14}$$

Here $\mathbf{E}$ denotes the expectation. The derivation of $\mathbf{c}_{ijk}$ is given in the Appendix and the matrices are sparse in nature due to the orthogonality of basis functions. The coefficients of the matrix $\mathbf{c}_{ijk}$ for the expansion (M = 5) are shown in Figure 6, where nnz is the number of non-zero elements. The

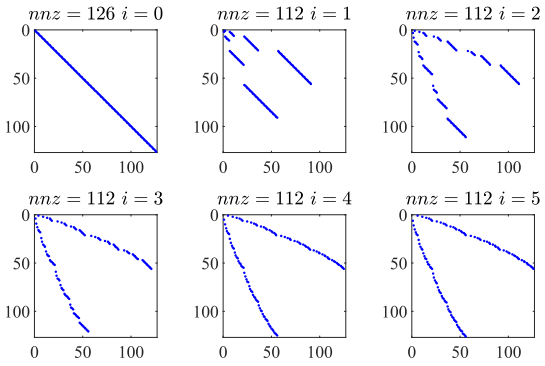

Figure 6. Coefficients of $\mathbf{c}_{ijk}$.

terms associated with i = 0 are the mean quantities. $\boldsymbol{T}_0 = \bar{\boldsymbol{T}}, \boldsymbol{S}_0 = \boldsymbol{S}$ and $\boldsymbol{F}_0$ represent the source term which is the current density. Finally, the second level of assembly is implemented, where the first $\boldsymbol{T}_{jk}$ matrices are computed and the terms associated to $\mathbf{c}_{ijk} \neq 0$ are only summed up and plugged

Prepared using jnmauth.cls
DOI: 10.1002/jnm

into the main matrix as shown in (15). In practice, there is no need to assemble the matrix. Here, however we have been content to use MATLAB default solver. However, $\boldsymbol{S}$ is expanded only to match the matrix dimension and does not contribute to the conductivity field expansion.

$$\begin{bmatrix} \boldsymbol{L}_{00} & \cdots & \boldsymbol{L}_{0,\mathrm{P\text{-}1}} \\ \boldsymbol{L}_{10} & \cdots & \boldsymbol{L}_{1,\mathrm{P\text{-}1}} \\ \vdots & \cdots & \vdots \\ \boldsymbol{L}_{\mathrm{P\text{-}1},0} & \cdots & \boldsymbol{L}_{\mathrm{P\text{-}1},\mathrm{P\text{-}1}} \end{bmatrix} \cdots \begin{bmatrix} \boldsymbol{a}_0 \\ \boldsymbol{a}_1 \\ \vdots \\ \boldsymbol{a}_{\mathrm{P\text{-}1}} \end{bmatrix} = \begin{bmatrix} \boldsymbol{F}_0 \\ 0 \\ \vdots \\ 0 \end{bmatrix} \tag{15}$$

The number of unknowns in the system (15) is n $\times$ P. The dimension of the matrix obviously depends on the number of nodes in the finite elements, the degree of the polynomial basis (p) and the number of terms needed to approximate the conductivity field.

3. RESULTS AND DISCUSSION

The equation system (15) was solved for different p at M = 5. The mean value and standard deviation obtained from SGFEM were compared with the Monte Carlo simulation as shown in Table II.

Table II. Mean and standard deviations of the interlaminar loss at 50 Hz

Method	Mean loss	Standard deviation	Computation time
MC	126.0583 W	13.232 W	3 hr 44 min
SGFEM at M = 5, p = 2	127.6256 W	13.512 W	14.25 min
SGFEM at M = 5, p = 3	127.2202 W	13.327 W	20.20 min
SGFEM at M = 5, p = 4	126.06166 W	13.291 W	52.92 min

Monte Carlo (MC) simulations were performed for 1000 realizations of random conductivities sampled using the random generator of MATLAB. The difference between these methods is that in MC method, the n $\times$ n matrix is solved for 1000 times whereas, in the SGFEM, the nP $\times$ nP sparse matrix is solved just once. Then, from the solutions of the magnetic vector potential, the eddy current loss was calculated. Based on the law of large numbers it can be stated that the

Prepared using jnmauth.cls
DOI: 10.1002/jnm

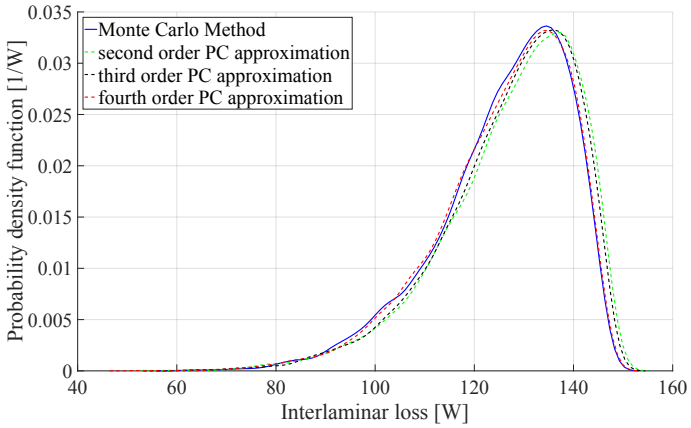

Figure 7. Probability density function of the interlaminar loss at 50 Hz.

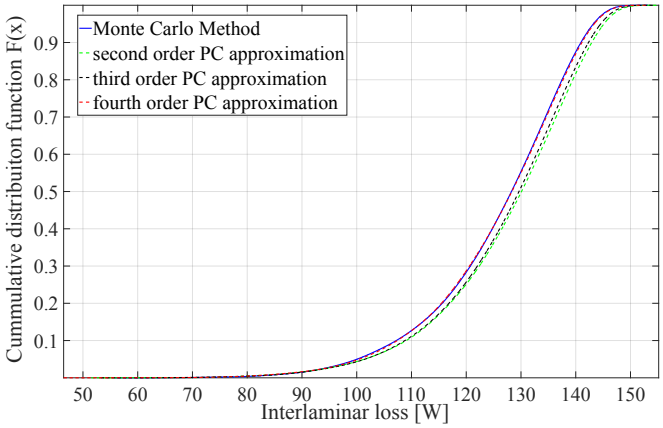

Figure 8. Cumulative distribution function of interlaminar loss at 50 Hz.

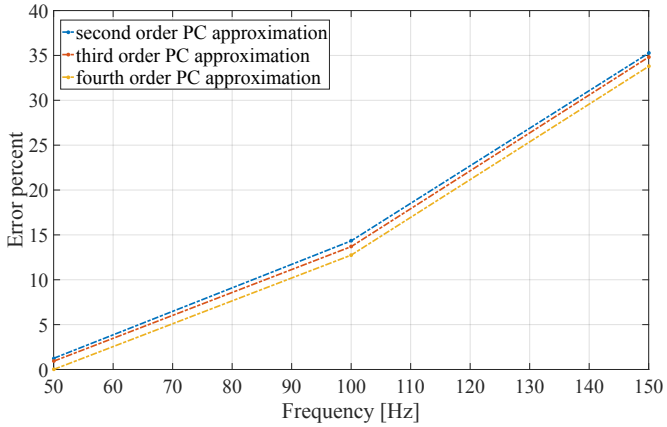

Figure 9. Error percentage compared to mean loss obtained from Monte Carlo method at different frequency.

Prepared using jnmauth.cls
DOI: 10.1002/jnm

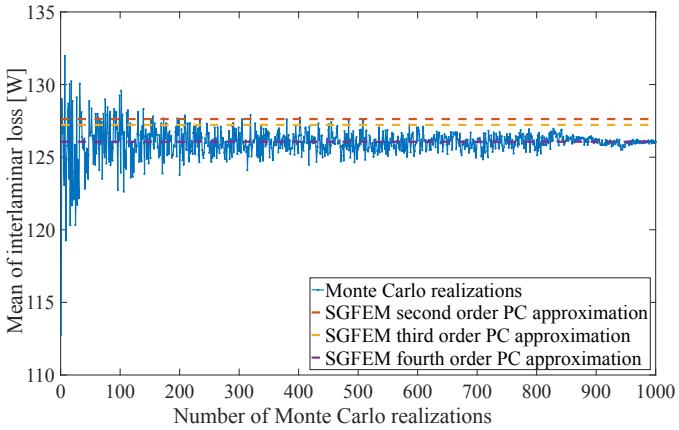

Figure 10. Comparison of convergence of MC and SGFEM at 50 Hz

Monte Carlo method converges almost surely to the expected value. The convergence of the Monte Carlo simulation is shown in Figure 10 and the expected values from SGFEM method are also compared. The probability density functions of the inter-laminar losses were also calculated using the solutions of both SGFEM and MC. It can be seen from Figure 7 and Figure 8 that at p = 4, SGFEM approximates close to MC. The investigation of different orders of the approximation, methods, accuracy and computation time is shown in Table II. The mean values of the interlaminar losses at different frequencies are also calculated and compared with the MC. The error is shown in Figure 9. It can be seen that as p increases, the error reduces, but the error increases as frequency increases. However, these simulations were performed at M = 5, so at higher frequencies, the number of expansion terms should be increased for better accuracy.

4. CONCLUSION

The paper presents an SGFEM to model the random interlaminar contacts and to estimate the interlaminar losses in electrical sheets. The SGFEM is computationally more efficient compared to the Monte Carlo method provided the algorithms have not been parallelized. The interlaminar loss obtained using the solutions of the proposed method is compared with the MC method, and a deviation of 1.3 % is obtained at 50 Hz at p = 2, M = 5 and a deviation of 1 % at p = 4 and M = 5

Prepared using jnmauth.cls
DOI: 10.1002/jnm

at 50 Hz. In this paper, the burr width parameter was chosen greater than what it occurs in reality for the sake of development of the model. The developed model can be directly implemented with a smaller burr width which requires a denser mesh and a more expensive computation. However, the method has been applied to quantify the uncertainty and its propagation through the magnetic vector potential formulation. The implementation of the SGFEM reduces the computation time compared to the MC method by 76 % with a deviation of 1 % at 50 Hz at p = 4 and M = 5. It strongly suggests that the SGFEM has faster convergence than the MC method. Hence, this approach is suitable for finite element optimization under uncertain parameters.

APPENDIX

The residual of (12) after substituting (8), (5) in (10),

$$\epsilon = \sum_{i=0}^{\mathrm{M}} \sum_{j=0}^{\mathrm{P\text{-}1}} \boldsymbol{S}_i \boldsymbol{a}_j \psi_j(\zeta_i(\theta)_{i=1}^{\mathrm{M}}) + \mathrm{j}\omega \sum_{i=0}^{\mathrm{M}} \sum_{j=0}^{\mathrm{P\text{-}1}} \boldsymbol{T}_i \boldsymbol{a}_j \psi_j(\zeta_i(\theta)_{i=1}^{\mathrm{M}}) - \boldsymbol{f}. \tag{16}$$

The approximation of the exact solution in the space spanned by $(\psi_k)_{\mathrm{k=1}}^{\mathrm{P\text{-}1}}$ by minimizing the residual which is equivalent to the condition that the residual to be orthogonal to space spanned by ψ_k [8], [26]. Finally, (16) is written as

$$\mathbf{E}[\epsilon \cdot \psi_k] = 0, \quad k = 0, \cdots \mathrm{P\text{-}1}. \tag{17}$$

The Jacobi polynomial on (a, b) with parameters $\alpha > 0$ and $\beta > 0$ is defined as ψ_j and ψ_k and the probability density function of the beta distribution with shape parameters $\alpha, \beta > 0$ is given by $\rho(\alpha, \beta, a, b)$. Then, the expectation is given by

$$\mathbf{E}[\zeta_i \psi_j \psi_k] = \int \psi_i \psi_j \rho(\alpha, \beta, a, b) \mathrm{d}x \tag{18}$$

ACKNOWLEDGEMENT

The research leading to these results has received funding from the European Research Council under the European Unions Seventh Framework Programme (FP7/2007-2013) ERC grant agreement no 339380. Paavo Rasilo acknowledges the Academy of Finland for financial support.

Prepared using jnmauth.cls
DOI: 10.1002/jnm

REFERENCES

1. Baudouin P, Wulf MD, Kestens L, Houbaert Y. The effect of the guillotine clearance on the magnetic properties of electrical steels. *Journal of Magnetism and Magnetic Materials* 2003; **256**(13):32 – 40, doi: 10.1016/S0304-8853(02)00004-5.
2. Hamzehbahmani H, Anderson P, Eldieb A. An overview of the recent developments of the inter-laminar short circuit fault detection methods in magnetic cores. *Power Engineering Conference (UPEC), 2015 50th International Universities*, 2015; 1–7, doi:10.1109/UPEC.2015.7339835.
3. Hamzehbahmani H, Anderson P, Jenkins K. Interlaminar insulation faults detection and quality assessment of magnetic cores using flux injection probe. *IEEE Transactions on Power Delivery* Oct 2015; **30**(5):2205–2214, doi:10.1109/TPWRD.2015.2413900.
4. Handgruber P, Stermecki A, Br O, Ofnery G. Evaluation of interlaminar eddy currents in induction machines. *Industrial Electronics Society, IECON 2013 - 39th Annual Conference of the IEEE*, 2013; 2792–2797, doi: 10.1109/IECON.2013.6699573.
5. R Mazurek HH, Moses AJ, Anderson P, Anayi FJ, Belgrand T. Effect of artifical burrs on local power loss in a three-phase transformer core. *IEEE Transaction on Magnetics* 2012; **48**:1653–1656.
6. Moses AJ, Aimoniotis M. Effects of artificial edge burrs on the properties of a model transformer core. *Physica Scripta* 1989; **39**(3):391. URL http://stacks.iop.org/1402-4896/39/i=3/a=025.
7. Roger JY, Vrignaud E, Henneron T, Benabou A, Ducreux J. Electromagnetic modelling of short circuited coreplates. *COMPEL - The international journal for computation and mathematics in electrical and electronic engineering* 2009; **28**(3):762–771, doi:10.1108/03321640910941016. URL http://dx.doi.org/10.1108/03321640910941016.
8. Sudret B, Kiureghian D. Stochastic finite elements and reliability: A state of the art report. *Technical Report Report UCB/SEMM-2000-08*, University of California 2000.
9. Gaignaire R, Clenet S, Sudret B, Moreau O. 3d spectral stochastic finite element method in electromagnetism. *Electromagnetic Field Computation, 2006 12th Biennial IEEE Conference on*, 2006; 6–6, doi:10.1109/CEFC-06.2006.1632799.
10. Wu W, Ni C. A study of stochastic fatigue crack growth modeling through experimental data. *Probabilistic Engineering Mechanics* 2003; **18**(2):107 – 118, doi:http://dx.doi.org/10.1016/S0266-8920(02)00053-X. URL http://www.sciencedirect.com/science/article/pii/S026689200200053X.
11. Kundu A, Adhikari S, Friswell MI. Stochastic finite elements of discretely parameterized random systems on domains with boundary uncertainty. *International Journal for Numerical Methods in Engineering* 2014; **100**(3):183–221, doi:10.1002/nme.4733. URL http://dx.doi.org/10.1002/nme.4733.
12. Gaignaire R, Clenet S, Moreau O, Sudret B. Current calculation in electrokinetics using a spectral stochastic finite element method. *IEEE Transactions on Magnetics* June 2008; **44**(6):754–757, doi:10.1109/TMAG.2008.915801.

Prepared using jnmauth.cls
DOI: 10.1002/jnm

13. Gaignaire R, Scorretti R, Sabariego R, Geuzaine C. Stochastic uncertainty quantification of eddy currents in the human body by polynomial chaos decomposition. *IEEE Transactions on Magnetics,* Feb 2012; **48**(2):451–454, doi:10.1109/TMAG.2011.2171925.

14. Ramarotafika R, Benabou A, Clenet S, Mipo JC. Experimental characterization of the iron losses variability in stators of electrical machines. *IEEE Transactions on Magnetics* April 2012; **48**(4):1629–1632, doi:10.1109/TMAG.2011.2173473.

15. Ramarotafika R, Benabou A, Clenet S. Stochastic modeling of soft magnetic properties of electrical steels: Application to stators of electrical machines. *IEEE Transactions on Magnetics,* Oct 2012; **48**(10):2573–2584, doi:10.1109/TMAG.2012.2201734.

16. Mac DH, Clnet S, Beddek K, Chevallier L, Korecki J, Moreau O, Thomas P. Influence of uncertainties on the b(h) curves on the flux linkage of a turboalternator. *International Journal of Numerical Modelling: Electronic Networks, Devices and Fields* 2014; **27**(3):385–399, doi:10.1002/jnm.1963. URL http://dx.doi.org/10.1002/jnm.1963, jNM-13-0076.

17. Beddek K, Le Menach Y, Clenet S, Moreau O. 3-d stochastic spectral finite-element method in static electromagnetism using vector potential formulation. *IEEE Transactions on Magnetics,* May 2011; **47**(5):1250–1253, doi:10.1109/TMAG.2010.2076274.

18. Rosenblatt M. Remarks on a multivariate transformation. *The Annals of Mathematical Statistics* 1952; **23**(3):470–472. URL http://www.jstor.org/stable/2236692.

19. Shah SB, Rasilo P, Belahcen A, Arkkio A. Estimation of additional losses due to random contacts at the edges of stator of an electrical machine. *COMPEL - The international journal for computation and mathematics in electrical and electronic engineering* 2015; **34**(5):1501–1510, doi:10.1108/COMPEL-02-2015-0083. URL http://dx.doi.org/10.1108/COMPEL-02-2015-0083.

20. Nayfeh AH. *Perturbation Methods*. Wiley-Interscience, 1973.

21. Liu WK, Belytschko T, Mani A. Random field finite elements. *International Journal for Numerical Methods in Engineering* 1986; **23**(10):1831–1845, doi:10.1002/nme.1620231004. URL http://dx.doi.org/10.1002/nme.1620231004.

22. Liu WK, Belytschko T, Mani A. Applications of probabilistic finite element methods in elastic/plastic dynamics. *Journal of Engineering for Industry* 1987; **109**:1087–1357.

23. Yamazaki F, Member A, Shinozuka M, Dasgupta G. Neumann expansion for stochastic finite element analysis. *Journal of Engineering Mechanics* 1988; **114**(8):1335–1354, doi:10.1061/(ASCE)0733-9399(1988)114:8(1335). URL http://dx.doi.org/10.1061/(ASCE)0733-9399(1988)114:8(1335).

24. Ghanem R, Spanos P. *Stochastic Finite Elements: A Spectral Approach*. Civil, Mechanical and Other Engineering Series, Dover Publications, 2003.

25. Raisee M, Kumar D, Lacor C. A non-intrusive model reduction approach for polynomial chaos expansion using proper orthogonal decomposition. *International Journal for Numerical Methods in Engineering* 2015; **103**(4):293–312, doi:10.1002/nme.4900. URL http://dx.doi.org/10.1002/nme.4900, nme.4900.

Prepared using jnmauth.cls
DOI: 10.1002/jnm

26. Leinonen M, Hakula H, Hyvnen N. Application of stochastic galerkin fem to the complete electrode model of electrical impedance tomography. *Journal of Computational Physics* 2014; **269**:181 – 200, doi:http://dx.doi.org/10.1016/j.jcp.2014.03.011. URL http://www.sciencedirect.com/science/article/pii/S0021999114001843.

27. Arkkio A. Analysis of induction motors based on the numerical solution of the magnetic field and circuit equations. G4 monografiavitskirja, Department of Electrical Engineering and Automation, Aalto University 1987-12-18. URL http://urn.fi/urn:nbn:fi:tkk-001267.

28. Zadehgol A, Cangellaris AC, Chapman PL. A model for the quantitative electromagnetic analysis of an infinitely long solenoid with a laminated core. *International Journal of Numerical Modelling: Electronic Networks, Devices and Fields* 2011; **24**(3):244–256, doi:10.1002/jnm.774. URL http://dx.doi.org/10.1002/jnm.774.

29. Schölkopf B. The kernel trick for distances. *Proceedings of the 13th International Conference on Neural Information Processing Systems*, NIPS'00, MIT Press: Cambridge, MA, USA, 2000; 283–289. URL http://dl.acm.org/citation.cfm?id=3008751.3008793.

30. Rahimi A, Recht B. Random features for large-scale kernel machines. *Advances in Neural Information Processing Systems 20*, Platt JC, Koller D, Singer Y, Roweis ST (eds.). Curran Associates, Inc., 2008; 1177–1184. URL http://papers.nips.cc/paper/3182-random-features-for-large-scale-kernel-machines.pdf.

31. Vedaldi A, Zisserman A. Efficient additive kernels via explicit feature maps. *IEEE Transactions on Pattern Analysis and Machine Intelligence* March 2012; **34**(3):480–492, doi:10.1109/TPAMI.2011.153.

32. Xiu D. *Numerical Methods for Stochastic Computations: A Spectral Method Approach*. Princeton University Press, 2010.

33. Beiler AC, Schmidt PL. Interlaminar eddy current loss in laminated cores. *Transactions of the American Institute of Electrical Engineers* Jan 1947; **66**(1):872–878, doi:10.1109/T-AIEE.1947.5059521.

Prepared using jnmauth.cls
DOI: 10.1002/jnm